Controlling spatio-temporal evolution of square and rectangular flames via inlet conditions

J. Stempka*, A. Tyliszczak*
Corresponding author: artur.tyliszczak@pcz.pl

* Faculty of Mechanical Engineering and Computer Science, Czestochowa University of Technology, Al. Armii Krajowej 21, 42-201 Czestochowa, Poland

Abstract: The paper focuses on the dynamics of turbulent hydrogen flames arising as the result of the mixing of a fuel jet issuing from rectangular nozzles and a hot co-flowing stream of oxidizer. We analyse the impact of the inlet conditions (an aspect ratio $AR = 1 - 5$, the Reynolds number $Re = 10\,000$ and $23\,600$, and a turbulence intensity $Ti = 2\%$ and 10%) on the flame characteristics along the axial direction and the radial directions along the minor and major axes of the nozzles. The research are performed applying large eddy simulation (LES) method and two numerical codes, ANSYS Fluent and an in-house high order SAILOR code. The so-called no-model approach is used for the combustion modelling, i.e., the reaction terms are computed directly based on the filtered quantities. It has been found that that the impact of the nozzle AR is the largest when the Reynolds number and turbulence intensity are small. In this case both the localization of the point where the temperature started to rise along the axis and the localization of its maximum values were significantly different. The differences in the temperature profiles were reflected by the profiles of the main species (hydrogen, oxygen and water mass fractions). We observed that depending on the Reynolds number and AR the flame stabilizes as attached or lifted.

Keywords: Turbulent Flames, Large-eddy Simulations, Flow Control.

1 Introduction

The flow control methods can be classified into two main groups, i.e., active and passive ones. The first one require sophisticated design, however, they allow to adjust the excitation to match broader range of flow conditions. They also need an input of energy for driving actuators with a required amplitude and frequency to provide variability of flow rate in order to get desirable dynamic flame response [1]. The passive methods are simpler to realise in practice and they rely on a geometrical shaping of flow domains (injector shapes, nozzles contraction, etc.) [2, 3] or addition of elements to the flow domain. During the operation of a given device, the passive approach does not require any additional energy input and is very efficient. The passive flow control methods are relatively inexpensive ways of obtaining desirable flow characteristics, leading for example to improved mixing processes. This feature is important in sophisticates flow system, especially in combustion, e.g., in burners, combustion chambers, boilers or engines where the mixing efficiency of reactants is critical. In this study we aim at the mixing process improvement by analysing the potential of passive flow control. By doing so we showed that one is able to adjust the combustion process characteristics, i.e., the flame lift-off height and other flames features in a desired and predictable manner. In previous studies focused on non-reacting jets [3] and flames [4] it has been demonstrated that by shaping the jet/fuel nozzle one can obtain significantly different flow dynamics. Compared to the classical circular jets or flames, it turns out that those emanating from non-circular nozzles naturally enhance mixing, particularly, large-scale mixing phenomena were found to be substantially intensified [2, 5]. In more recent work of Tyliszczak and Geurts [6] devoted to jets, it has been shown that changing an AR of rectangular nozzle, one can substantially change the jet spreading rate, amplify the vortices growth and even cause the bifurcation phenomenon.

In the present work we analyse sensitivity of the hydrogen diffusion flames to change in the inlet conditions, including: (i) the inlet velocity (Reynolds number); (ii) varying aspect ratio of a nozzle, $AR = 1$, 2, 3 and 5; (iii) the inlet turbulence intensity, i.e., $Ti = 2\%$ and 10%. As shown in [6], in case of isothermal constant density rectangular jet flows the first two parameters influence a global jet dynamics, whereas the third one affects a small-scale mixing provided that the Reynolds number is relatively small. In the present investigations we analyse to what extent these findings translate to the flame dynamics.

The computations are performed applying the large eddy simulation (LES) method. We use both a high-order in-house numerical code and also a commercial ANSYS Fluent software. For combustion modelling we applied the Eulerian stochastic field (ESF) approach coupled with a detailed chemical scheme of hydrogen combustion. The obtained results confirm the ability to enhance the mixing process of the fuel and oxidizer and thus the combustion process by changing the nozzle AR through appropriate modulation the sizes and time scales of emerging turbulent structures. This in turn allows obtaining the different flame characteristics like a lift-off height or length of the flame and the fuel conversion rate.

2 Problem Description

The conditions and composition of the investigated jet flames are similar to those studied by Cabra et al. [7]. The fuel jet is composed of hydrogen ($X_{H_2} = 0.25$) and nitrogen ($X_{N_2} = 0.75$) while its temperature is equal to $T_j = 305\ K$. It mixes with a hot co-flowing oxidizer ($T_{cf} = 1045\ K$, $X_{O_2} = 0.15$, $X_{H_2O} = 0.1$, $X_{N_2} = 0.75$) and auto-ignites at some distance downstream the nozzle. In the current study we consider rectangular jets with the aspect ratios $AR = L/h = 1$, 2, 3 and 5, where L and h are the dimensions of the nozzle exit highlighted in Fig. 1b). In all the cases the cross-sectional areas S are the same and correspond to a circle with the diameter $D_e = 2\sqrt{S/\pi} = 4.57\ mm$. We consider the jets characterized by two Reynolds number values, $Re = U_b D_e/\nu = 10\,000$ and $23\,600$, where U_b is the bulk velocity and ν is the kinematic viscosity of the fuel. Changing the aspect ratio plays a role of the passive flow control method in the current study.

3 Numerical Approach

3.1 Flow Modelling

The applied modelling method is based on a low Mach number approximation of Navier-Stokes equations. For chemically reacting cases we additionally solve a set of the transport equations for species, and the transport equation of specific enthalpy. These are complemented with the equation of state. A full flow model takes the following form [8]:

$$\partial_t \overline{\rho} + \nabla \cdot (\overline{\rho} \widetilde{\mathbf{u}}) = 0, \tag{1}$$

$$\overline{\rho} \partial_t \widetilde{\mathbf{u}} + (\overline{\rho} \widetilde{\mathbf{u}} \cdot \nabla) \widetilde{\mathbf{u}} = -\nabla \overline{p} + \nabla \cdot (\tau + \tau^{sgs}), \tag{2}$$

$$\overline{\rho} \partial_t \widetilde{Y}_\alpha + \overline{\rho} \widetilde{\mathbf{u}} \cdot \nabla \widetilde{Y}_\alpha = \nabla \cdot \left(\overline{\rho} \left(D_\alpha + D_\alpha^{sgs} \right) \nabla \widetilde{Y}_\alpha \right) + \overline{\rho \dot{\omega}}_\alpha, \tag{3}$$

$$\overline{\rho} \partial_t \widetilde{h} + \overline{\rho} \widetilde{\mathbf{u}} \cdot \nabla \widetilde{h} = \nabla \cdot \left(\overline{\rho} \left(D + D^{sgs} \right) \nabla \widetilde{h} \right), \tag{4}$$

$$p_0 = \overline{\rho} R \widetilde{T}, \tag{5}$$

where $\mathbf{u}$, Y_α, h represent the velocity vector, mass fraction of $\alpha = 1, ..., N$ species and specific enthalpy, respectively. The LES filtered variables are denoted by bar symbol whereas Favre filtered variables are indicated by the tilde. Symbols ρ, p, p_0, R, D_α, D and τ represent the density, hydrodynamic and thermodynamic pressure, gas constant, species mass and heat diffusivities and the viscous stress tensor. The sub-grid stress tensor $\tau^{sgs} = 2\mu_{sgs}\mathbf{S}$ is modelled based on a sub-grid viscosity μ_{sgs} and the rate of strain tensor $\mathbf{S}$. The τ^{sgs} was calculated differently depending on the stage of the simulations, i.e., the results from the first stage of simulations (see section 3.3) were obtained using the WALE model [9] while the Vreman model [10] was used in the second stage of computations.

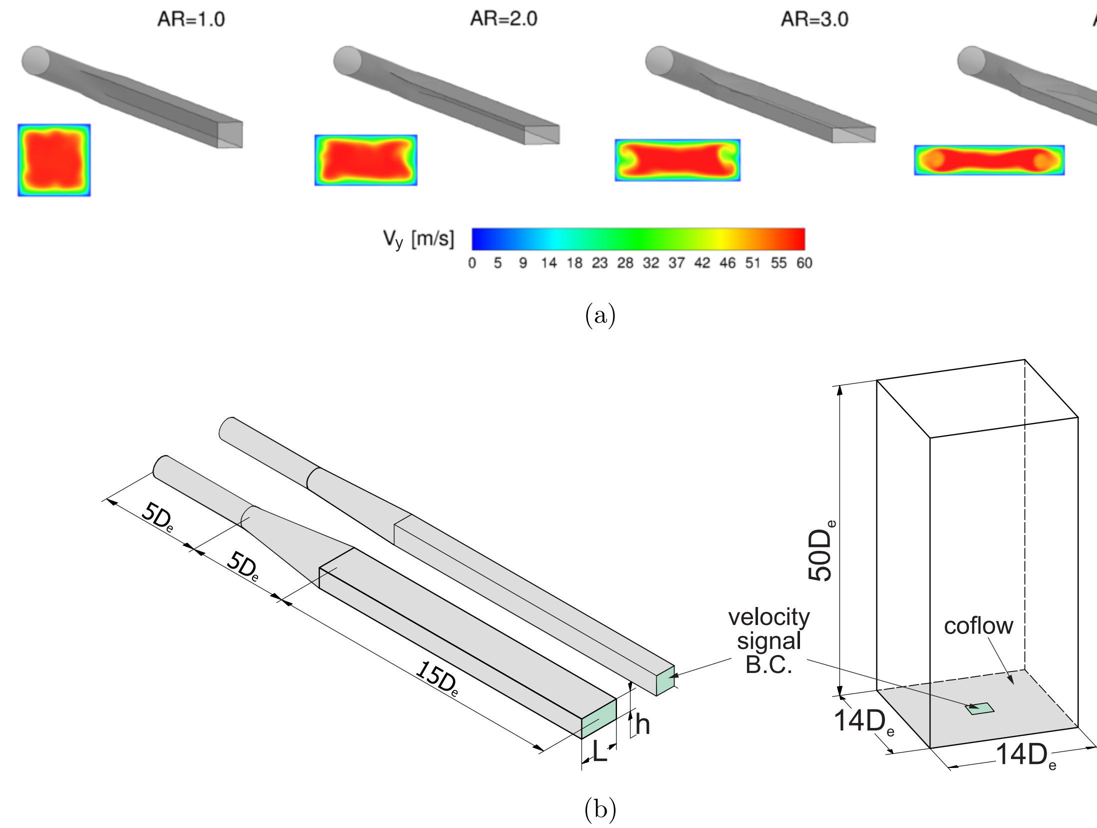

Figure 1: Schematic of the numerical setup (a) and nozzle geometries with the axial velocity distributions at the exit plane for the case with $Ti = 2\%$ and $Re = 10\,000$.

3.2 'No model' approach for the combustion modelling

Modelling of a combustion process can be realized by applying a number of models, e.g., flamelet, thickened flame, conditional moment closure, Eulerian stochastic field, etc. In this work we performed a series of time consuming simulation and therefore the applied model had to be a compromise between the accuracy and efficiency. For this reason we applied the so-called 'no model' approach in which the reaction source terms in (3) are computed directly based on the filtered quantities as

$$\overline{\dot{\omega}_\alpha(\mathbf{Y}, h)} \approx \dot{\omega}_\alpha(\widetilde{\mathbf{Y}}, \widetilde{h}) \tag{6}$$

and this means that the impact of the sub-filter unresolved scales is neglected. The 'no model' assumptions would certainly fail in the Reynolds Averaged Navier-Stokes (RANS) framework as the fluctuations in RANS models are large in general. On the other hand, in the laminar flows and in DNS of turbulent flows, where all flow scales are resolved, the 'no model' approach is perfectly valid. Hence, one may assume that for a sufficiently dense computational mesh, when the sizes of cells are of the order of the Kolmogorov length scale, the use of this method is appropriate. The correctness of the 'no model' approach was verified in [11, 12, 13].

3.3 Numerical procedure

The simulations were performed in two stages. In the first one, we modelled the flow developing inside the nozzles with variable cross-sections. Each nozzle ended as a rectangle with different AR (see Fig. 1a,b). In this stage, the simulations were carried out using ANSYS Fluent software [14], applying the WALE subgrid-scale viscosity model. At the same time, the unsteady velocity values from the outlets of the nozzles were acquired. Examples of the instantaneous signals in terms of the axial velocity distributions at the nozzles exit planes are presented in Fig. 1a. It can be clearly seen that the AR impacts on the internal flow structures and thus the outlet velocity. The recorded signals were then used as the inlet boundary conditions in the second stage of simulations. They were imposed on a bottom plane of a rectangular computational domain for the second part of the computational procedure, as schematically presented in Fig. 1b,c). At this stage, the computations were carried out using an in-house LES solver SAILOR. This code is based on the 6th order compact difference scheme on half-staggered meshes [15]. The time integration is performed applying predictor-corrector approach with the Adams-Bashforth and Adams-Moulton methods. The Vreman model [10] is used for the sub-grid viscosity. The chemical reactions are computed using CHEMKIN interpreter [16] and the detailed mechanism of Mueller [17] involving 9 species and 21 reactions. The reaction terms are stiff and therefore they are integrated in time applying operator splitting approach and the VODPK [18] solver that is suitable for stiff systems. The accuracy of the SAILOR code and the applied modelling approach for the test cases similar to the present ones were verified in simulations of non-reacting square jets [3] and also for the Cabra flame [7] in a paper [4]. In the performed simulations the computational domain was discretized using $192 \times 192 \times 384$ mesh points in the radial and axial directions, respectively. The mesh points were compacted radially towards the nozzle region and axially towards the inlet boundary. Preliminary tests have shown that the solutions obtained on the applied mesh are practically independent on the mesh density.

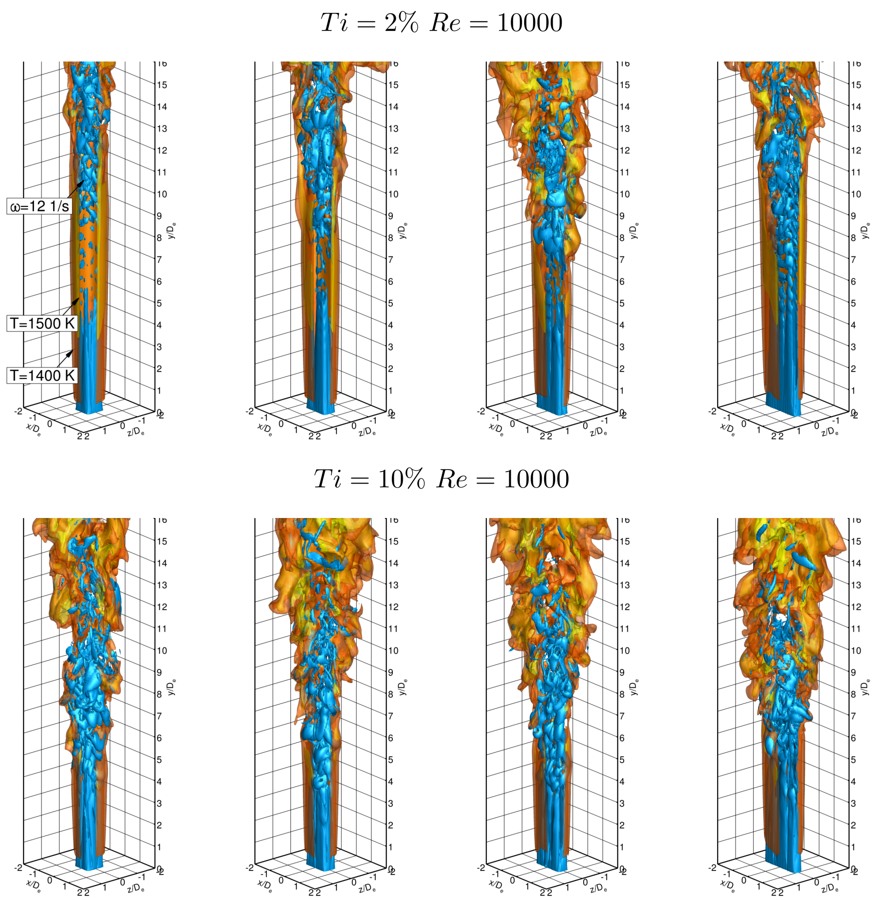

(a) $AR = 1.0$ (b) $AR = 2.0$ (c) $AR = 3.0$ (d) $AR = 5.0$

Figure 2: Instantaneous iso-surfaces of two temperature values, $T = 1400$ K, $T = 1500$ K, and vorticity $|\omega| = 12$ s^{-1} for the cases at $Re = 10\,000$.

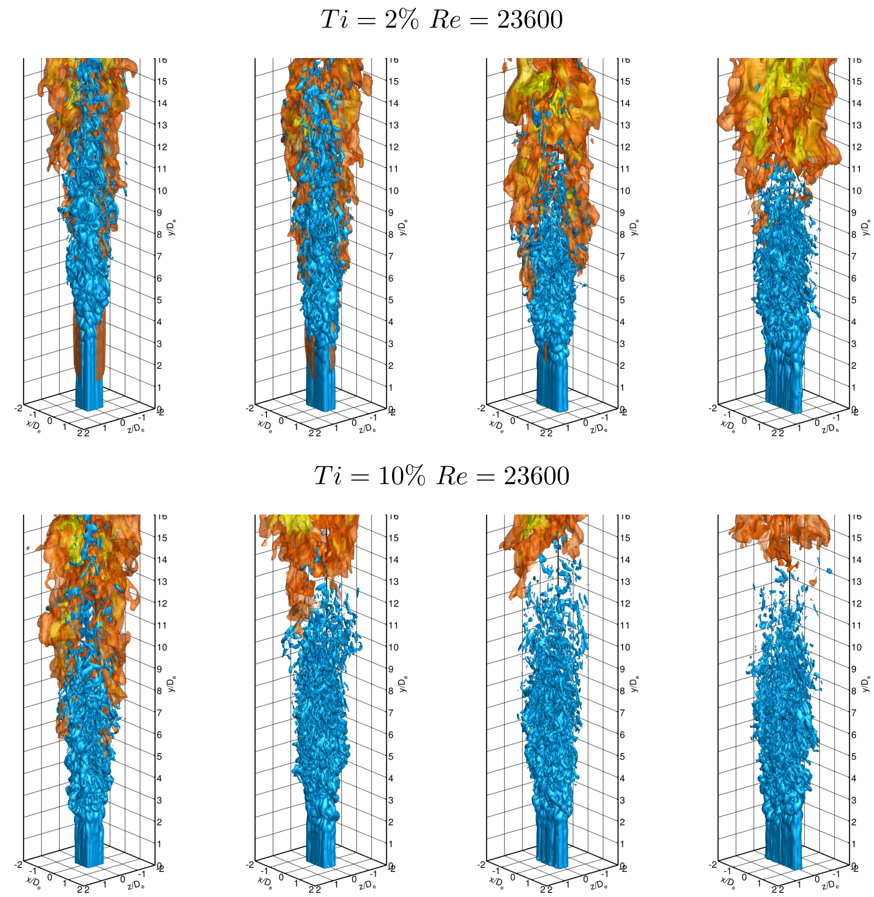

(a) $AR = 1.0$ (b) $AR = 2.0$ (c) $AR = 3.0$ (d) $AR = 5.0$

Figure 3: Instantaneous iso-surfaces of two temperature values, $T = 1400$ K, $T = 1500$ K, and vorticity $|\omega| = 12$ s^{-1} for the cases at $Re = 23\,000$.

4 Results

4.1 Flame structure

First we analyse qualitatively the instantaneous 3D flame structure of all analysed cases. Figures 2 and 3 show the instantaneous iso-surfaces of two temperature values, i.e., $T = 1400$ K, $T = 1500$ K, and the vorticity module $|\omega| = 12\,\mathrm{s}^{-1}$. It is evident that the flames are sensitive to the change of boundary conditions. Regarding the influence of the turbulence intensity it can be seen that its change form $Ti = 2\%$ to $Ti = 10\%$ makes the flame structures more complex and more turbulent as one could expect. For $Re = 10000$ the flames are attached to the nozzle (see Fig. 2) and in these cases the change of Ti seems to affect their structure only far from the inlet. On the other hand, for the larger Reynolds number, the flames are lifted and the lift-off height (L_h) for $Ti = 10\%$ is longer. In these cases also the influence of AR is the most pronounced. One can observe that L_h increases not only with T_i but also with the increasing AR.

4.2 Time-averaged results

In this section we analyse time-averaged result of the main parameters characterizing the flames. Figure 4 shows the distributions of time-averaged temperature in the 'x-y' cross-section plane in the center of the computational domain ($z = 0$). The black iso-line represents the stoichiometric mixture fraction $Z_{st} = 0.476$. It can be seen that its axial localization extends downstream the most for the case with $AR = 1$. It decreases

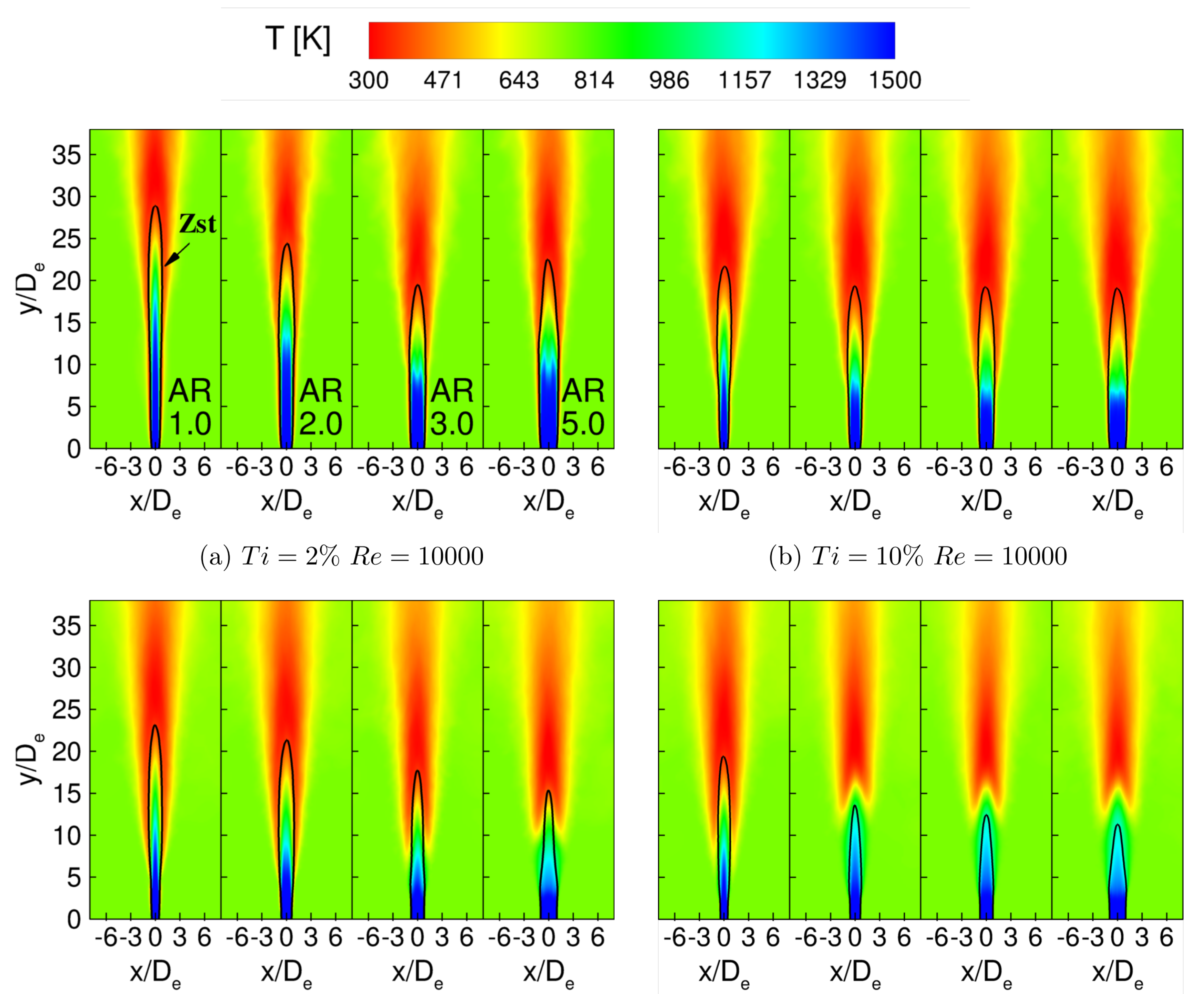

(a) $Ti = 2\%$ $Re = 10000$ (b) $Ti = 10\%$ $Re = 10000$

(c) $Ti = 2\%$ $Re = 23600$ (d) $Ti = 10\%$ $Re = 23600$

Figure 4: Planar distributions of time-averaged temperature in the 'x-y' cross-section plane in the center of the computational domain ($z = 0$). The black iso-line represents the stoichiometric mixture fraction $Z_{st} = 0.476$.

for the larger Reynolds number and Ti. Also when the AR increases the Z_{st} line moves closer to the nozzle. The only exception is the case with $Ti = 2\%$ and $Re = 10\,000$ where for $AR = 5$ the axial localization of Z_{st} is longer than for $AR = 3$. Taking account the temperature distributions, it can be seen that for $Re = 10\,000$ the flame occurs in the mixing layer in the region close to the nozzles. For $Re = 23\,600$ the situation is different and in these cases the flame positions depend both on Ti and AR. Regarding the impact of AR, the significant differences are seen for the cases with $Ti = 2\%$. For $AR = 1$ and $AR = 2$ the flames appear in the mixing layer and are almost attached, while for $AR = 3$ and $AR = 5$ they are visibly lifted and their anchoring points move downstream, particularly for $AR = 5$. For $Ti = 10\%$ the temperature distributions in the flames issuing from the rectangular nozzles seem very similar. In the next sections we examine its values along the axial and radial directions.

4.3 Axial statistics

In Fig. 5 the axial profiles of $\langle T \rangle$, $\langle Y_{H_2} \rangle$, $\langle Y_{H_2O} \rangle$, $\langle Y_{O_2} \rangle$ are presented. The hydrogen mass fraction can be regarded as an indicator of the potential core length (L_p) and it can be assumed as a measure of a penetration distance along which the fuel does not mix with the co-flowing stream. For $Re = 10\,000$ and $Ti = 2\%$ for

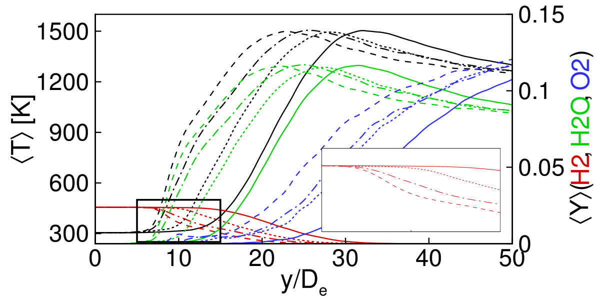

(a) $Ti = 2\%$ $Re = 10000$

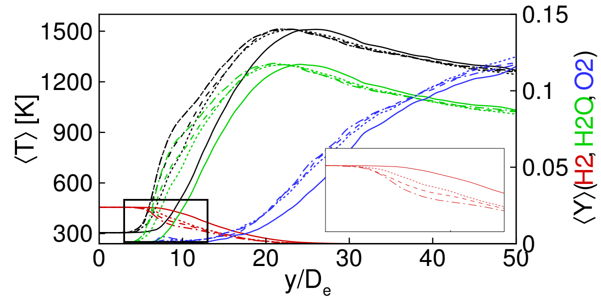

(b) $Ti = 10\%$ $Re = 10000$

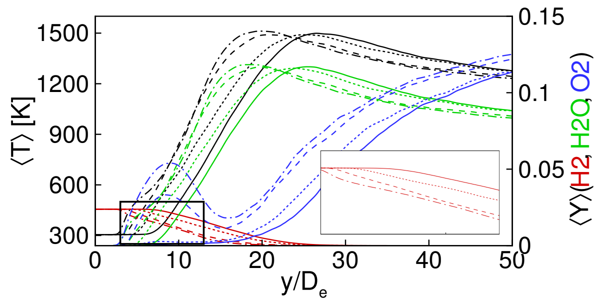

(c) $Ti = 2\%$ $Re = 23600$

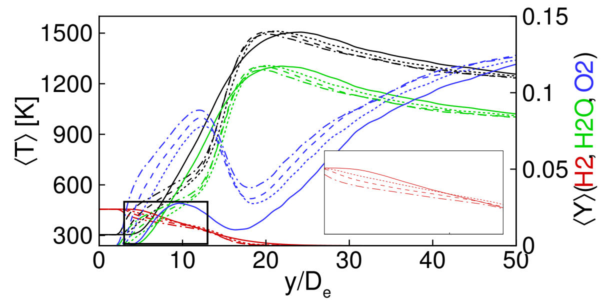

(d) $Ti = 10\%$ $Re = 23600$

Figure 5: Axial profiles of the selected quantities, i.e., $\langle T\rangle$, $\langle Y_{H_2}\rangle$, $\langle Y_{H_2O}\rangle$, $\langle Y_{O_2}\rangle$. Legend: (——) $AR = 1.0$, (⋯⋯) $AR = 2.0$, (- - -) $AR = 3.0$, (-·-·-) $AR = 5.0$.

which the influence of AR is the largest, it can be seen that L_p extends up to $y/D_e \approx 12$ for $AR = 1$ and then gradually decreases to $y/D_e \approx 7.5$ for $AR = 3$. These localizations can be directly related with the points where the temperature starts to grow. Note that initially the increase of the temperature and the values of $\langle Y_{H_2O}\rangle$ and $\langle Y_{O_2}\rangle$ are not due to combustion process but only because of the mixing with the hot co-flowing stream. As the point where the combustion begins in the axis ($L_{h,a}$) we assume the location where the temperature is 1% higher than the oxidizer temperature. For $Re = 10\,000$ and $Ti = 2\%$ this point lies in between $y/D_e \approx 10$ for $AR = 3$ and $y/D_e \approx 20$ for $AR = 1$. Worth noticing is that for $AR = 1$ and $AR = 2$ the slopes of the temperature profiles in the region upstream of the occurrence of its maximum value does not change, while for $AR = 3$ and $AR = 5$ it becomes less steep starting from $L_{h,a}$. The same is found for the $\langle Y_{H_2O}\rangle$ profiles.

For $Re = 10\,000$ and $Ti = 10\%$ there are visible differences between the solution obtained for the case with the nozzle with $AR = 1$ and the remaining cases. However, considering the differences due to AR it can be seen that they are much smaller than for $Ti = 2\%$. The maxima of the temperature are shifted upstream but their localizations for $AR = 2$, 3, 5 are practically the same. The differences between the profiles of the species mass fractions are also small, especially if one takes into account the profiles of $\langle Y_{O_2}\rangle$.

The scenario is different for the flames at $Re = 23\,600$. At first, it can be seen that L_p is definitively shorter and it varies in between $y/D_e \approx 4-7$ for $Ti = 2\%$ and $y/D_e \approx 3-4$ for $Ti = 10\%$. Additionally, one can observe a significant initial entrainment of O_2 to the axis region. On should also note that the profiles of $\langle Y_{O_2}\rangle$ are influenced by the nozzle geometry. For $Ti = 2\%$, after an initial quick rise of $\langle Y_{O_2}\rangle$ for $AR = 3$ and $AR = 5$ it drops down significantly. For $Ti = 10\%$ this happens for all the cases and is accompanied by a linear growth of the temperature and $\langle Y_{H_2O}\rangle$ of which profiles are characterized by significantly different slopes in the regions $y/D_e \approx 6-12$ and $y/D_e \approx 12-19$.

4.4 Radial statistics

Figure 6 presents the radial profiles of $\langle T\rangle$, $\langle T'T'\rangle$ and $\langle Y_{OH}\rangle$ taken from different axial locations ($y/D_e = 2$, 4, 8, 12, 16, 20, 24 and 30) along the semi-major and semi-minor symmetry axis of the nozzles. They show

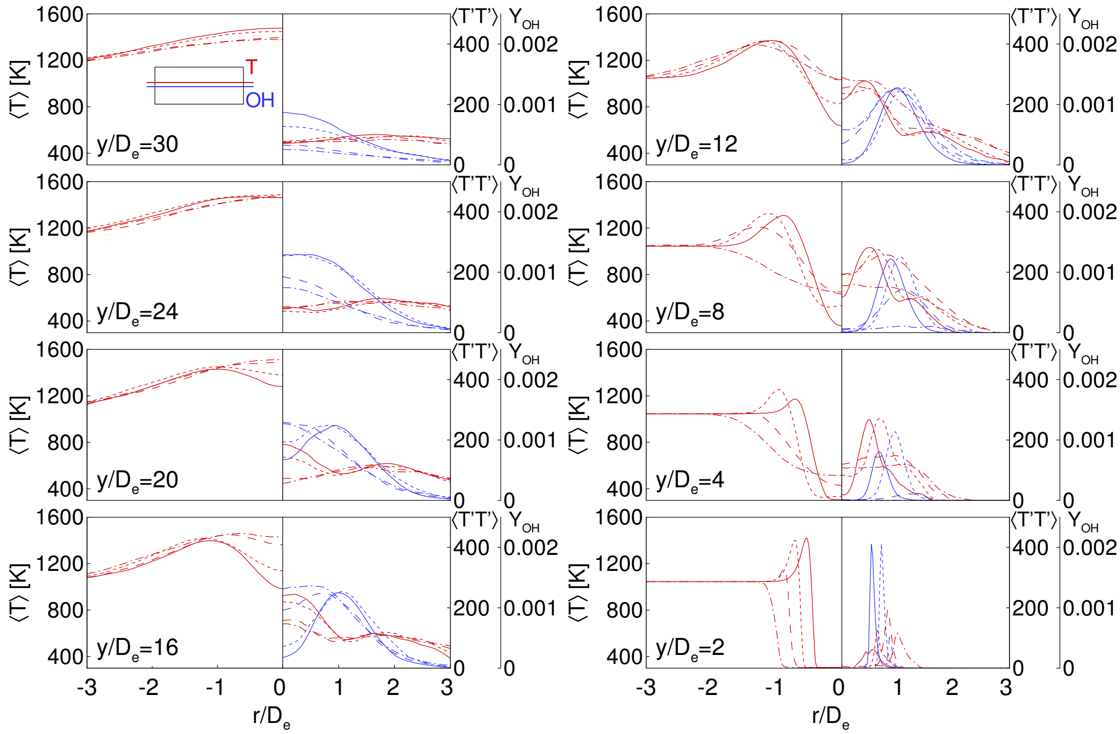

(a) semi-major axis, $Ti = 2\%$ $Re = 23600$

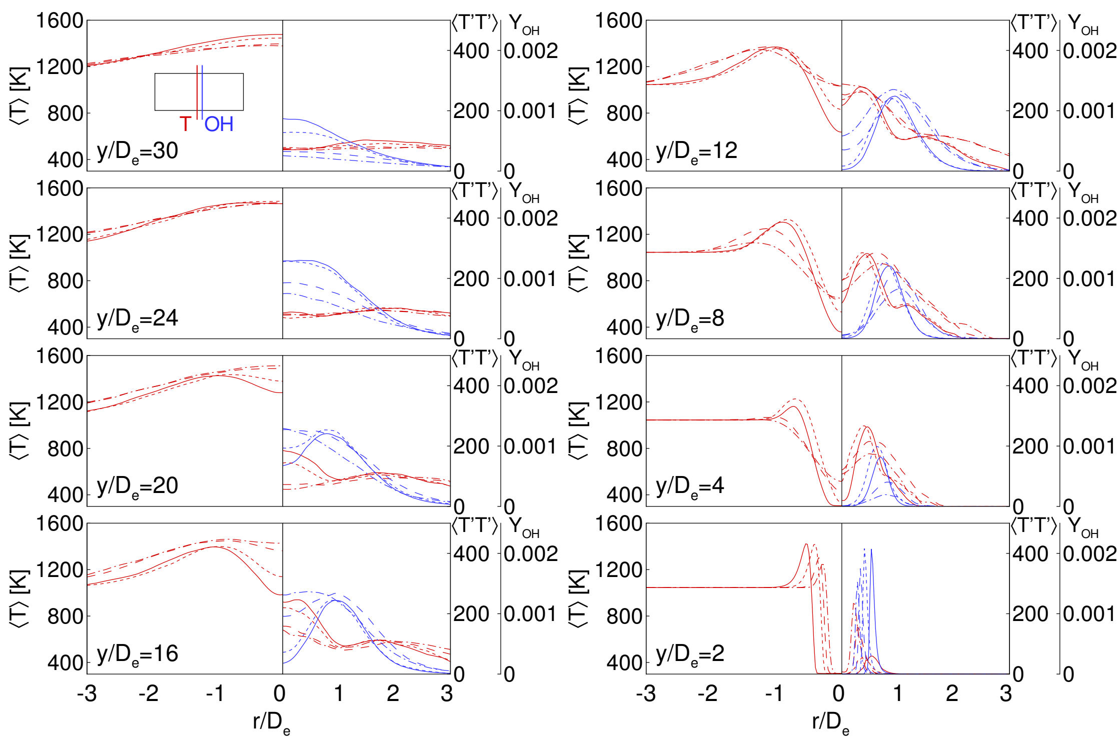

(b) semi-minor axis, $Ti = 2\%$ $Re = 23600$

Figure 6: Radial profiles of selected quantities, i.e., $\langle T \rangle$, $\langle T'T' \rangle$ and $\langle Y_{OH} \rangle$ taken from different axial locations (y/D_e = 2, 4, 8, 12, 16, 20, 24 and 30) along the semi-major and semi-minor symmetry axis of the nozzle. Legend: (——) $AR = 1.0$, (⋯⋯) $AR = 2.0$, (- - -) $AR = 3.0$, (-·-·-) $AR = 5.0$.

the variability of the flame with respect to the long side of the nozzle in Fig. 6a) and the short side in Fig. 6b). Only the results for the cases with $Re = 23\,600$ and $Ti = 2\%$ are presented.

They show clearly that the flame structure is non-homogeneous in azimuthal direction. For example the solutions in Fig. 6 indicate that the flame issuing from the nozzle with $AR = 5.0$ starts to develop at the distance almost $8D_e$ faster along the short side than along the long one. This is confirmed by higher values of $\langle T \rangle$ and $\langle Y_{OH} \rangle$ found along the minor symmetry axis, which suggests that the auto-ignition appears faster. This fact can be partially explained by the fact that the hot co-flowing gas is transported in a higher rate toward the jet along the short side.

Starting from the location $y/D_e = 24$ the profiles of the mean values and fluctuations of temperature are almost the same irrespectively on the nozzle AR. Only the radical $\langle Y_{OH} \rangle$ profiles show different levels. Non-zero values in the cases with $AR = 1.0$ and 2.0 suggest that the combustion process is further from equilibrium than for higher AR jets, as non-negligible amount of fuel prevails further downstream.

5 Conclusions

This paper presented the results of LES of hydrogen diffusion flames issuing from square and rectangular nozzles. The research concentrated on the influence of the initial conditions (the Reynolds number $Re = 10\,000\,23\,600$, turbulence intensity $Ti = 2\%$, 5%, nozzle aspect ratio $AR = 1$, 2, 3, 5) on the flame characteristics. Both the instantaneous and time averaged results were presented. The latter along the axial and two radial directions along the minor and major nozzle axes. It has been shown that the impact of the nozzle aspect ratio is the largest when the Reynolds number and turbulence intensity are small. In this case both the localization of the point where the temperature started to rise along the axis and the localization of its maximum values were significantly different. It has been shown that the flames issuing from the nozzles with $AR = 1$, 2 are attached, while those issuing from the nozzles with $AR = 3$, 5 are lifted. For $Re = 23\,600$ we observed that the impact of AR on the flame behaviour in the axis was pronounced only for the cases with $Ti = 2\%$. For $Ti = 10\%$ the solutions obtained for the nozzle with $AR = 1$ differed from the ones obtained for $AR = 2$, 3, 5, but differences between the latter were very small. Analysis of the flame along the radial directions along the minor and major nozzle axes revealed a significant flame inhomogeneity. It has been shown that the flame appears closer to the nozzle in the mixing layer region, which is initially perpendicular to the minor nozzle axis.

Acknowledgements

This work was supported by the National Science Center in Poland (Grant 2018/31/B/ST8/00762) and the statutory funds of the Department of Thermal Machinery (Czestochowa University of Technology). The authors wish to acknowledge Prof. Bernard J. Geurts for his valuable suggestions that helped us in achieving the results presented in this paper. This collaboration was possible thanks to the ANIMATE project (Grant no. PPI/APM/2019/1/00062/DEC/01) funded by the Polish National Agency for Academic Exchange. The computations were carried out using PL-Grid infrastructure.

References

[1] T. Schuller, T. Poinsot, and S. Candel. Dynamics and control of premixed combustion systems based on flame transfer and describing functions. *Journal of Fluid Mechanics*, 894, 2020.

[2] E. J. Gutmark and F. F. Grinstein. Flow control with noncircular jets. *Annual Review of Fluid Mechanics*, 31(1):239–272, 1999.

[3] A. Tyliszczak, Ł. Kuban, and J. Stempka. Numerical analysis of non-excited and excited jets issuing from non-circular nozzles. *International Journal of Heat Fluid Flow*, 94:108944, 2022.

[4] Ł. Kuban, J. Stempka, and A. Tyliszczak. Numerical analysis of the combustion dynamics of passively controlled jets issuing from polygonal nozzles. *Energies*, 14(3):554, 2021.

[5] C. B. da Silva and O. Métais. Vortex control of bifurcating jets: A numerical study. *Physics of Fluids*, 14(11):3798–3819, 2002.

[6] A. Tyliszczak and B. J. Geurts. Controlled mixing enhancement in turbulent rectangular jets responding to periodically forced inflow conditions. *Journal of Turbulence*, 16(8):742–771, 2015.

[7] R. Cabra, J. Chen, R. Dibble, A. Karpetis, and R. Barlow. Lifted methane–air jet flames in a vitiated coflow. *Combustion and Flame*, 143(4):491–506, 2005.

[8] B. J. Geurts. *Elements of Direct and Large Eddy Simulation.* R.T. Edwards, Inc, 2003.

[9] F. Nicoud, H. B. Toda, O. Cabrit, S. Bose, and J. Lee. Using singular values to build a subgrid-scale model for Large Eddy Simulations. *Physics of Fluids*, 23(8):085106, 2011.

[10] A. W. Vreman. An eddy-viscosity subgrid-scale model for turbulent shear flow: Algebraic theory and applications. *Physics of Fluids*, 16(10):3670–3681, 2004.

[11] C. Duwig, K. J. Nogenmyr, C. Chan, and M. J. Dunn. Large Eddy Simulations of a piloted lean premix jet flame using finite-rate chemistry. *Combustion Theory and Modeling*, 15(4):537–568, 2011.

[12] Prasad V.N., Juddoo M., Kourmatzis A., and Masri A.R. Investigation of lifted flame propagation under pulsing conditions using high-speed OH-LIF and LES. *Flow, Turbulence and Combustion*, 93(3):425–437, 2014.

[13] Agnieszka Wawrzak and Artur Tyliszczak. A spark ignition scenario in a temporally evolving mixing layer. *Combustion and Flame*, 209:353–356, 2019.

[14] *ASYS Fluent User's Guide, Release 19.5, ANSYS, Inc.*

[15] A. Tyliszczak. A high-order compact difference algorithm for half-staggered grids for laminar and turbulent incompressible flows. *Journal of Computational Physics*, 276:438–467, 2014.

[16] CHEMKIN-PRO, Reaction Design: San Diego, CHEMKIN Software.

[17] M.A. Mueller, T.J. Kim, R.A. Yetter, and F.L. Dryer. Flow reactor studies and kinetic modeling of the H2/O2 reaction. *International Journal of Chemical Kinetics*, 31(2):113–125, 1999.

[18] P.N. Brown and A.C. Hindmarsh. Reduced Storage Matrix Methods in Stiff ODE Systems. *Journal of Applied Mathematical Computations*, 31:40–91, 1989.